Projection of lightning over South/South East Asia using CMIP5 models

Sagarika Chandra[a], Praveen Kumar[a], Devendraa Siingh[a]*, Indrani Roy[b], Jeni Victor N[a],

A. K. Kamra[a]

[a]Indian Institute of Tropical Meteorology, Pune, Ministry of Earth Science, India

[b]University College London, Gower Street, London, WC1E6BT, UK

***corresponding author**

Indian Institute of Tropical Meteorology,

Pashan, Pune-411008, India.

devendraasiingh@tropmet.res.in; devendraasiingh@gmail.com

Abstract

Product of Bowen ratio with the sum of precipitation rate and evaporation rate has been used as proxy to evaluate the seasonal and annual spatial distributions of lightning flash rate over South/Southeast Asian region (60–120° E, 0–40° N) with 9 models from the Coupled Model Inter-comparison Project-Phase 5 (CMIP5). The model-simulated mean LFR with each model is positively correlated with the satellite-observed LFR on both seasonal and annual scales. The satellite-observed LFR is correlated with the ensemble mean LFR of the models with a correlation coefficient of 0.93 over the region. The model-simulated LFR has also been used for projection of lightning in the late twentyfirst century. Overall, the projected LFR over whole study area shows a 6.75% increase during the (2079–2088) period in high radiative forcing scenario (RCP8.5) as compared to the historic period of (1996–2005). Rise in LFR is also identified using another projected period (2051–2060) and a lower radiative forcing scenario condition (RCP4.5), though lesser in magnitude, as expected. For the projected period (2051–60) in the RCP8.5 case, LFR over the domain shows an increase of 4.3%; whereas for a lower future scenario condition (RCP4.5), it indicates a rise by 5.36% at the end of the twenty-first century. Moreover, results indicate an increase in extreme events of severe convective storms with intense lightning in mountainous dry regions at the end of the twenty-first century. It is suggested that the proxy used here is favourable for projection of LFR in this region and perhaps for the whole tropical area.

Keywords: Bowen ratio, CMIP5, Evaporation, Lightning flash density, Precipitation

1. Introduction

Occurrence of lightning discharges in a thundercloud is closely related with its microphysical and dynamical characteristics of thundercloud (e.g., Vonnegut 1963; Williams et al. 1989, 1992; Zipser and Lutz 1994; Stolzenburg et al. 1998; Siingh et al. 2011; Cecil et al. 2015) and the environmental properties (e.g., Orville et al. 2001; Williams et al. 2002; Zipser et al. 2006; Stolz et al. 2015, 2017; Wu et al. 2016; Saha et al. 2017; Etten-Bohm et al. 2021) in which the cloud develops. In turn, as the cloud electrification develops, its electrical properties interact with the microphysical and dynamical characteristics through some feedback processes (e.g., Vonnegut 1963; Kamra 1970, 1975, 1982a, b; Bala and Kamra 1991; Kamra et al. 1993). In addition, topography and land-use patterns of the region are well known to influence the lightning activity (e.g., Ramesh Kumar and Kamra 2012, Oulkar et al. 2019; Kamra and Penki 2021). As a consequence, lightning activity shows large spatio-temporal variability on the global as well as regional scales. The continental area of South/Southeast Asia hosts the World`s highest mountain peak in the Himalayas and the Tibetan plateau, the Thar desert and forested areas, experiences high rainfall in the monsoon season and undergoes large variability in the meteorological/environmental conditions; high temperature and convective activity, in particular (Houze et al. 2007). Consequently, large lightning variability is observed in this area and has been widely studied (e.g., Kandalgaonkar et al. 2005; Ranalkar and Chaudhari 2009; Dwivedi et al. 2014; Siingh et al. 2013, 2014, 2015; Saha et al. 2019; Kamra and Penki 2021; Qie et al. 2021). The area accounts for some of the World's hotspots of lightning (Albrecht et al. 2016).

Prediction of lightning is important to avoid the risk to the life and property, and to assess its impact on upper tropospheric chemistry and forest fires (Krause et al. 2014). However, because of the complex nature of its occurrence and distribution in a region, as discussed above, weather and climate models have not been so far able to successfully simulate and predict the lightning distribution in a region. Therefore, several attempts have been made to parameterize or use proxies to predict and project the lightening activity using different climate models (Tost et al. 2007; Finney et al. 2014; Clark et al. 2017). Recently, Romps et al. (2018) used the proxy of product of convective available potential energy (CAPE) and precipitation (P), suggested by Romps et al. (2014), to replicate and forecast lightning over the Contiguous United States (CONUS). This proxy could explain 77% of the variance of cloud-to-ground lightening flash rate over the CONUS during the 2011 calendar year. However, extending the analysis over a longer period of 2003-2016, Tippett et al. (2019) showed that the proxy performs better on diurnal and monthly scales but not so on semi-annual and annual scales. Moreover, the performance of the proxy is better only in cool seasons and not so in warm season when most of the lightning occurs over CONUS. Recognising the role of the sensible heat flux in modifying the buoyancy and lightning, Toumi and Qie (2004) argued that a product of Bowen ratio (BR) and precipitation (P) can act as a proxy for lightning over the Tibetan Plateau and explain the spring anomaly and annual variability of the lightening flash rate (LFR) in that region.

Despite an impressive performance of the (CAPE× P) in CONUS (Romps et al. 2014) and (BR × P) at the Tibetan Plateau (Toumi and Qie 2004), both proxies show a weak correlation with LFR in the tropical land area of (0-40 °N, 60-120 °E) (South/Southeast Asia including some part of South China) (Chandra et al. 2021; here in after referred as C21). Because of the high temperatures prevailing in the tropics, the surface heat fluxes and evaporation rate are large and considerably add to the moisture and convective instability of the atmosphere (Berg et al. 2013). Consequently, LFR in that area is likely to be largely affected by such factors. Based on such arguments, C21 proposed that product of Bowen ratio and sum of precipitation rate (Pr) and evaporation rate (Er) i.e. BR (Pr + Er), can serve as a proxy to study the variability of LFR in this area. This proxy could explain 90% of the variance in LFR and had the maximum correlation with LFR among the 9 proxies examined by C21. In this paper, we use the proxy BR (Pr + Er) developed by C21 to test the performance of 9 CMIP5 climate models and their ensemble mean in simulating the spatial distribution of LFR on the seasonal and annual scales. These models incorporating this proxy have also been used for projection of the LFR distribution and its change in this area by the end of 21^{st} century.

2. Data and methodology

The lightning flash rate data used in this study are obtained from the space-borne optical sensors merged product of Lightning Imaging Sensor (LIS) and Optical Transient Detector (OTD) mounted on the Tropical Rainfall Measuring Mission (TRMM) satellite. The daily LIS/OTD data of Low Resolution Time Series (LRTS) of version 2.3 available in the grid resolution of 2.5°×2.5° for the period of 1996–2005 were downloaded (http://thunder.msfc.nasa.gov/data/data_lis. tml) for the Southeast Asian region (0 °N-40 °N and 60 °E-120 °E). Subsequently this data were rescaled to 0.5°×0.5° and used for spatial distribution. Precipitation rate, evaporation rate, surface air temperature, sensible heat flux and latent heat flux with grid resolution of 0.5°×0.5°, were obtained from the improved version of European Centre for Medium-Range Weather Forecasts (ECMWF), ERA5 reanalysis products (https://cds.climate.copernicus.eu).

Simulated precipitation rate (P_r), air temperature (T), and evaporation rate (E_v) are obtained from the Coupled Model Inter-comparison Project Phase 5 (CMIP5, http://cmip-pcmdi.llnl.gov/cmip5/) data archive. CMIP5 is a coordinated effort among international climate modelling groups to simulate past, present, and future climate to better understand the response of the climate system to human and natural perturbations to energy balance (Taylor et al. 2012). An earlier work (Jourdain et al. 2013) selected 9 specific CMIP5 models and showed spatial pattern of observed Indian Summer Monsoon (ISM) rainfall was captured reasonably well in those models. In the Indian context, other studies, however, did extensive analysis focusing on 23 selected CMIP5 models for (Roy and Tedeschi 2016; Roy, Gagnon and Siingh 2019; Roy, Tedeschi and Collins 2017, 2019 ; Roy 2017).

Those showed major findings remain the same if the ensemble mean of 23 models is used instead of those specific 9 models, in particular. Hurwitz et al. (2014) selected a few from the set of those particular nine models and added a few more to explore other regions of the globe too and showed their main results were consistent in their chosen sets of models. In this work, a total of nine models are evaluated (CANESM2, CNRM-CM5, FGOALS-G2, GFDL-CM3, GFDL-ESM2M, GFDL-ESM2G, MIROC5, MIROC5-ESM-CHEM and MIROC5-ESM). Models are selected as per the availability of all required parameters alongside those were previously chosen by other studies being better performing models, as discussed earlier (Jourdain et al. 2013; Roy and Tedeschi 2016; Roy et al 2017; Roy, Gagnon and Siingh 2019; Roy 2017; Hurwitz et al. 2014). To understand future scenarios, we use data of CMIP5, Representative Concentration Pathways 8.5 scenario (RCP 8.5) documented in Riahi et al. (2011). Recent research also analysed those models in the Indian context using RCP8.5 scenarios (Roy, Tedeschi and Collins 2019, Roy 2018). In this study, the years 1996-2005 of the CMIP5 "historical" experiment represent the current climate, while the years 2079-2088 of the "RCP8.5" experiment are used to represent the late 21st century climate. We consider the 10 years data (1996-2005) for the historic period from models, therefore we choose all the meteorological and LFR data of this period for the observational study. We mainly considered the highest radiative forcing scenario RCP8.5, to capture maximum detectable signals. The higher end of the future scenario (2079-2088) is chosen to identify larger changes. However, results were also tested for another projected period (2051-60) and a lower radiative forcing scenario condition, RCP 4.5.

In order to simulate the spatial distribution of LFR with different models, we use the relation, LFR = K × BR(Pr + Er) where LFR is the density of lightning flash rate in flashes km^{-2} day^{-1}, P_r is the precipitation rate in kg m^{-2} day^{-1}, E_r is the evaporation rate in kg m^{-2} day^{-1}. Using the fact that 1 mm of precipitation equals 1 kg m^{-2} of liquid water, therefore, here precipitation rate has been taken in kg m^{-2} day^{-1} instead of mm day^{-1}. BR, the Bowen ratio (ratio of sensible heat flux to latent heat flux), is a dimensionless quantity and its magnitude describes the energy gained or lost from the earth surface to the atmosphere. K is the proportionality constant with units as number of flashes per kilogram of water. C21 evaluated the value of K = 1.25, 0.1, 0.9 and 0.8 kg m^{-2} day^{-1} for the pre-monsoon, monsoon, post-monsoon and winter seasons respectively with an annual mean of K =1.1 kg m^{-2} day^{-1}.

3. Results and Discussion

3.1. Seasonal variation of derived LFR

Spatial distributions of LFR evaluated from nine GCMs' outputs using our lightning proxy for the historic period (1996-2005) in different seasons are presented in **Figure 1 (a-d)**. Top panels show the observed LFR (left) and the ensemble mean of nine selected models (right), rest other panels show the simulated LFR from the nine different models.

Observed LFRs during the pre-monsoon season (MAM) **(Figure 1a)** are intensified in the north-eastern and north-western regions of India as well as in the Indo-Gangetic basin along the foothills of the southern Himalayan foothills (SHF)s. It is also high in the maritime continents (includes Indonesia, Philippines and Papua New Guinea) and mainland Southeast Asia (the continental portion of Southeast Asia that includes Thailand, Cambodia, LAOS, Vietnam). All those parts are captured well by models (**Figure 1(a)).** Maximum signature is noticed around Gangetic West Bengal and Bangladesh. Those regions are highly affected by Nor'westers during the pre-monsoon season (Tyagi et al. 2011, 2013; Dwivedi et al. 2014), which bring a lot of moisture from the nearby ocean and form thunderclouds with lightning flashes. Topography of the Himalayan mountain ranges restrain high surface temperature interacting with the prevailing wind and moisture supply from the Bay of Bengal which is favourable for the genesis of convection and formation of lightning along the southern Himalayan foothills (SHF) (Houze et al. 2007; Qie et al. 2014; Wu et al. 2016). The moisture over the Bay of Bengal is driven from northward to the eastern SHF by the southwesterly wind during the pre-monsoon; hence, intense convective systems (ICSs) mainly occur over the eastern SHF. In the onset of monsoon, maximum water vapor is transported northwestward along the Himalayas and extending to the middle of the SHF due to enhancement of oceanic southwesterly winds. Higher values of the observed LFR in the north-eastern part of the Himalayan regions are clearly visible in top left panel for ensemble mean of all the models in **Figure 1(a)**. Penki and Kamra (2013) also reported that the northeast part of the Himalaya gets maximum LFR during the pre-monsoon season. The model-simulated LFR using our proxy well captures its intensification in this region. C21 also reported that spatial distribution of the observed LFR in the north-eastern part of the Himalaya matches well with the spatial distribution of the proxy BR (Pr+Er). On the other hand maritime continents and mainland Southeast Asia get higher concentration of flashes during this season which is well captured in all models and clearly noticeable from the spatial distribution of observed data. These maritime and mainland continents are noted as the hotspots of South/Southeast Asia (Albrecht et al. 2016). The models such as CANESM2, FGOALS-G2, GFDL series and MIROC5 show a good association with the observed spatial distribution of LFR (**Figure 1(a)**). Some of the models however overestimate signature in regions of mainland Southeast Asia (GFDL models, MIROC5-ESM-CHEM and MIROC5-ESM) which are liable to give strong signature around that region in ensemble mean (**Figure 1a**, top right).

The southwest monsoon or Asian monsoon season (JJAS) plays a crucial role in the occurrence of deep convection over some parts of the south/southeast Asian region (Qie et al. 2014). In the monsoon season, the north-western part of India and north Pakistan especially Himalayan region has the maximum LFR as compared to the other parts of the study region (**Figure 1b).** The southern slopes of the Himalayan range have highly intensified LFR (Ramesh Kumar and Kamra 2012), since this region holds intense convection due to establishment of water vapour transport passage from the Bay of Bengal along the Himalayan foothills to the west. After the Indian summer monsoon establishes, the southwesterly wind over the ocean is strongest, and the warm and moist air flowing from the Arabian Sea arrives and brings moisture at the western end of the transport route along the SHF. It encounters the warm and dry air from Afghan high lands at mid-tropospheric level and the moist air from the Bay of Bengal. This, along with orography and surface heating of the region, results in convective instability and formation of most of the ICSs in monsoon being concentrated at the concave indentation of the westernmost SHF (Liu et al. 2020). Wu et al. (2013, 2016) investigated that the occurrences of ICS along the SHF mainly occurs during March-October, and their maximum monthly frequency appears in May, while the deep convective systems over the Northwestern Himalaya occur in July. Moreover, severe convection tends to occur in regions with a sharp moisture gradient at the lower atmosphere. That region of strongest signature is also well captured by the model-derived LFR and comparable with the observed LFR as shown in the top left panel of **Figure 1 (b)**. CANESM2, GFDL-CM3, GFDL-ESM2G and GFDL-ESM2M models shows better agreement with observation. Models of MIROC5 series though capture some regional features well but overestimate in few locations.

The post-monsoon (ON) season is influenced by the northwest monsoon; moreover, the wind pattern is different from that of the monsoon season. The convective activity is less as compared to the pre-monsoon and monsoon seasons. Inspite of some divergence, all the nine models and their ensemble roughly capture the observed LFR spatial pattern (**Figure 1(c)**). The models CANESM2, FGOALS-G2 and MIROC5 are performing better over others. Observed strong signature around Maritime continent is however missing in all models and hence missed in ensemble mean too. Similar to the post-monsoon season, lightning activity in the winter season in this region is weak as shown in **Figure 1(d).** This season does not show much of lightning due to calm, dry and cold weather and the consequent low convective activity. The maritime islands such as Indonesia and Sumatra are affected most in the observed LFR. The signature in foothills of Himalayas is captured well by all models using our proxy; however, signature in maritime continent seems weak.

Thus, our analyses of spatial distribution pattern of LFR using derived proxy of C21 indicate that the models are usually capturing seasonal variations reasonably well. Focusing on scaling of LFR shows that maximum signature is noticed during pre-monsoon (upper bound 0.132) followed by monsoon (0.12), post-monsoon (0.06) and winter (0.05) respectively. Foothills of the Himalayas are seen prone to thunderstorm activity in all seasons. In the Indian context, Northwest India is experiencing maximum LFR in monsoon and post-monsoon, while Gangetic west Bengal and Bangladesh during pre-monsoon. All these seasonal variations in spatial patterns are well-captured by individual models and their ensemble using the proxy of C21.

3.2. Annual variation of derived LFR

Figure 2 shows the annual mean of the LFR spatial distributions simulated by the 9 different models and their ensemble mean along with the annual mean of the observed LFR. The annual mean of the LFR simulated from all the nine GCMs' matches well with the annual mean of the observed LFR in the regions of intense lightning in the Himalayan regions and its foothills, the continental parts of south-east Asia and maritime islands. LFR over Gangetic West Bengal is also well captured by the annual mean from all models. These regions have already been earmarked as the lightning hotspots of the World (Albrecht et al. 2016).

Figure 3 shows a scatter plot of the monthly averaged values of LFR from the ensemble mean of GCMs' and the observed LFR over the whole study region for the period of 1996-2005. A strong positive correlation coefficient (R = 0.93) has been found between the monthly-averaged observed and simulated LFR for the period of 1996-2005. The correlation coefficients between the observed LFR and the simulated LFR from all the different models on seasonal and annual scale for the historic period (1996-2005) have been determined by Pearson's correlation method and are given in **Table 1**. The correlations determined for the CANESM2, FGOALS-G2, GFDL series and MIROC5 models are strong. Last two models from MIROC5 series in **Table 1**, correlate moderately in some seasons with the observed LFR, and these two models also overestimate. LFR over Tibetan plateau region as discussed in Section 3.1. The simulated LFR using this proxy and the observed LFR shows very good correlations during all the four seasons as well as on the annual scale over the study region.

3.3. Future projection of LFR

In view of the large changes in the meteorological and environmental conditions projected in the global warming scenario by the end of the 21st century, a corresponding change in the lightning distribution on regional and global scales is expected. Projecting such change is of importance not only for our understanding of the change, but also for the future planning. We have used our data to simulate LFR for the late 21st century over this region as compared to the historic period (1996-2005). In the future scenario of LFR for late 21st century (2079-2088), the top two panels in **Figure 4** show the annual ensemble mean of derived LFR (left) and the difference in LFR between the historic period and the annual simulated mean of the models at the end of the 21st century assuming the Representative Concentrations Pathway-8.5 (RCP-8.5) scenario (right). Other nine panels in **Figure 4** show the annual mean of derived LFR from the individual model for the future period. Most of the models also project that the major hotspots of LFR in the Himalayan region and foothills of Himalaya appear as well in the future as in the historic period. The top right panel of **Figure 4** shows that the north-western part of Himalayan region is likely to undergo the maximum enhancement of LFR as compared to other parts of the study region which suggests that, this part of the study region need be of highest concern in future period. The continental parts of the Southeast Asia, the Tibetan plateau and some parts of southern India are also likely to experience some enhancement in lightning activity. However, some regions, little south of the Himalayan foothills may experience a little reduction in lightning activity. Maritime continent also project a decrease in LFR from the historic period on annual scale.

Figure 5 shows the spatial distributions of LFR projected by ensemble means (left column) and the difference in LFR in RCP8.5 from the historical period (right column) in different seasons. It brings out dramatic differences in the projected LFR in different regions among different seasons. In the pre-monsoon season, LFR is projected to greatly increase in the northeast India and the southern continental parts of the south-east Asia. On the other hand, LFR is projected to undergo a general decrease but is marked with small areas of intense increase over the northwest India. This trend in LFR in the northwest area is projected more emphatically, both in magnitude and the covered area, in the monsoon season and will be discussed in more detail in the next paragraph. No appreciable change is projected in Himalayan foothills, northeast India and southern parts of the Indo-China peninsula. Some parts of the southern India and continental south-east Asia are projected to have enhanced LFR and a mild decrease is projected in the southern India in the monsoon season. Other noticeable features are a projected increase in LFR above the northwest of India in the monsoon season and an appreciable decrease in LFR over the Tibetan plateau in the winter season.

The observed and ensemble values of LFR in **Figure 1** and **2** show reasonably good agreement on seasonal and annual scales and their monthly-averaged values are correlated with a correlation coefficient of 0.93 (**Figure 3**) in historic period (1996-2005). An examination of the annual and seasonal spatial distributions of LFR in **Figures 4 and 5** leads to an important conclusion that if the ensemble LFR is low, the projected LFR in late 21st century is expected to decrease or not undergo any significant change. However, if the ensemble LFR is high, the projected LFR will increase in late 21st century. This amounts to supporting the prediction of an increase in the extreme events, severe convective storms in this case, in the global warming scenario (Trapp et al. 2007a, b; Diffenbaugh et al. 2013; Seeley and Romps 2015). Intensive increase in LFR in small areas in the pre-monsoon, monsoon and post-monsoon seasons in the northwest India and some other places indicate formation of severe convective storms producing intense lightning. Existence of meteorological conditions and complex topography of the north-western region of India is suitable for development of severe convective storms even in the historic period of 1996-2005 (Liu et al. 2020). Formation of thunderstorms in this area is reported to occur at sharp moisture gradients and along the lid of edge created by warm dry air above moist air at lower levels (Wu et al. 2016; Liu et al. 2020). The change in frequency and severity of such storms under different meteorological, environmental and topographical conditions during 21st century in global warming scenario has already been projected at some places (e.g., Price and Rind 1994; Trapp et al. 2007a, b; Kunkel et al. 2013; Seeley and Romps 2015).

The above discussion on projection of LFR by the end of 21st century in different seasons in this area leads us to conclude that LFR is likely to increase in moist regions, such as northeast India and southern Indo-China peninsula in the pre-monsoon season. However, in dry regions such as over complex topography of northwest India. LFR is projected to decrease but develop some isolated small areas of intense lightning in the pre-monsoon and post-monsoon seasons; with increasing trend in spatial extent of such isolated areas in the monsoon season. Moreover, over Tibetan plateau, LFR is projected to decrease in its northern part in winter and increase in southern part in hot season of pre-monsoon. However, overall increase in LFR by the end of 21st century in the whole study area on annual scale is projected to be 6.75% of the historic period (**Table 2**). Models such as CNRM-CM5 and GFDL models capture the variation of LFR well for the future scenario.

Changes in precipitation, evaporation and atmospheric temperature projected for the end of 21st century from the historic period widely differ from model to model (**Table 2).** However, ensemble mean of all the GCMs considered in this study, project that the precipitation, evaporation and temperature will increase with a mean increase of approximately 11%, 10% and 3.5% respectively by the end of 21st century over whole study region, **(Table 2).** Therefore, in a global warming scenario, the precipitation is expected to increase by ~3.5 % per °C and evaporation to increase by ~3 % per °C, over South/Southeast Asian region. However, the global precipitation has been expected to increase by ~ 2 % per Kelvin in future scenario (Lambert and Web 2008; Jeevanjee and Romps 2018). Using the method of percentage change between the years 1996-2005 and 2079-2088, ensemble mean of all GCMs predict that the annual mean LFR is expected to increase in South/Southeast Asia by 6.75%**.** However, past estimates for the future changes in LFR in the global warming scenario vary over a wide range and indicate both an increase or decrease in lightning activity (e.g., Williams et al. 1992; Price and Rind 1994; Tost et al. 2007; Clark et al. 2017; Finney et al. 2018). Romps et al. (2014) also estimated the annual mean of cloud-to-ground lightning strikes for the years of 2079-2088 of the RCP8.5 experiment over CONUS region increase upto ~ 12% per ºC of mean global temperature.

To check whether LRF shows a continuous increasing trend or not, we also considered another 10-year projected period (2051-60) in between (Table 3a), instead of the earlier projected period 2079-2088, as shown in Table 2. In terms of annual mean LFR, the ensemble mean of all GCMs over the same Asian domain indicates an increase by 4.3%, which is lower than the previous estimate (6.75%). Like Table2, MIROC5 and MIROC-ESM are shown giving low estimates compared to rest other models. Projected changes in precipitation, evaporation and temperature also suggest an increase for all models (Table 3a).

To further check how different future scenarios affect results, we analyzed the RCP4.5 scenario too (Table 3b). Like Table 2, projected period of 2079-2088 (with respect to the historic period 1996-2005) is considered. Ensemble mean of all GCMs again indicates a rise in LFR and estimates an increase by 5.36% (lower than RCP8.5 scenario). In terms of individual models, here also MIROC5 is identified as poor performing model.

4. Summary

A newly defined proxy for LFR is tested for CMIP5 models in historic period and used for prediction in future scenarios. Based on the 10 years of historic period analysis (1996-2005) from nine GCMs model data, the seasonal and annual variation of LFR is derived from the defined proxy and compared with the observed LFR from LIS/OTD. Models are shown well capturing the spatial pattern of LFR distribution in South/Southeast Asian region using this new proxy. Monthly mean simulated from ensemble of all models is correlated with the monthly mean of observed LFR with a correlation coefficient of 0.93. Overall, using RCP8.5 scenario, the GCMs predict a 6.75% increase in the LFR in the South/Southeast Asia over the end of 21st century. The rise in LFR is also identified using another projected period and a different future scenario condition. Considering a different 10-year projected period (2051-60) for the RCP 8.5 scenario, the ensemble mean of all GCMs over the same Asian domain indicates an increase in the LFR by 4.3%, which is, as expected, lower than the previous estimate (6.75%). The projected change in the LFR, using another future scenario condition

(RCP 4.5), also estimates an increase at the end of the 21st century, which is by 5.36% (lower than the RCP 8.5 scenario, as expected). Moreover, extreme events of severe convective storms with intense lightning in mountainous dry regions may increase in global warming scenario.

Acknowledgements

Indian Institute of Tropical Meteorology, Pune is funded by Ministry of Earth Sciences (MoES), Government of India. Authors are acknowledge the World Climate Research Programme's Working Group on Coupled Modelling, which is responsible for CMIP, and we thank the climate modelling groups (their respective models are listed in **Table 2**of this paper) for producing and making available their model output. The authors are thankful to NASA and ECMWF for providing the LIS-OTD data through their websites https://ghrc.nsstc.nasa.gov/lightning/data/data_lis_otd-climatology and https://cds.climate.copernicus.eu/ . AKK acknowledges Indian National Science Academy for the support under INSA Emeritus Scientist Programme.

Authors' contributions

SC, DS and AKK are responsible for inception and, execution of project and preparation of the draft of the manuscript. SC and PK analyzed and simulate the CMIP5 data and prepared the final figures. IR contributes towards the CMIP5 model for the projection of LFR. SC, DS and JV contributed towards the analysis and interpretation of the study. AKK prepared final draft of manuscript. All authors contributed to the discussion of the results.

Declaration of competing interests

The authors declare that they have no competing interests.

References

Albrecht RI, Goodman SJ, Buechler DE, Blakeslee RJ, Christian HJ (2016) Where Are the Lightning Hotspots on Earth?. Bull Amer Meteor Soc 97:2051–2068. https://doi.org/10.1175/BAMS-D-14-00193.1

Bala SS, Kamra AK (1991) Change in precipitation drag due to thunderstorm electrification. Atmos Res 26: 377-387.

Berg P, Moseley C, Haerter JO (2013) Strong increase in convective precipitation in response to higher temperatures. Nature Geosci 6:181-185.

Cecil DJ, Buechler DE, Blakeslee RJ (2015) TRMM LIS climatology of thunderstorm occurrence and conditional lightning flash rates. J Clim 28:6536–6547.

Chandra S, Siingh D, Victor NJ Kamra AK (2021) Lightning activity over South / Southeast Asia : Modulation by thermodynamics of lower atmosphere. Atmos Res 250:105378. doi:10.1016/j.atmosres.2020.105378

Clark SK, Ward DS, Mahowald NM (2017) Parameterization-based uncertainty in future lightning flash density. Geophy Res Lett 44(6): 2893-2901.

Diffenbaugh NS, Scherer M, Trapp RJ (2013) Robust increases in severe thunderstorm environments in response to greenhouse forcing. Proc Nat Aca Sci 110(41):16361-16366.

Dwivedi AK, Chandra S, Kumar M, Kumar S, Kiran Kumar NVP (2014) Atmospheric surface layer responses to the extreme lightning day in plateau region in India. J Atmos Solar-Terrestrial Phys 120:143–149. https://doi.org/10.1016/j.jastp.2014.08.003.

Etten-Bohm M, Yang J, Schumacher C, Jun M (2021) Evaluating the relationship between lightning and the large-scale environment and its use for lightning prediction in global climate models. J Geophys Res Atmos 126(5):2020JD033990.

Finney DL, Doherty RM, Wild O, Stevenson DS, MacKenzie IA, Blyth AM (2018) A projected decrease in lightning under climate change. Nat Clim Chang 8 (3):210–213. https://doi.org/10.1038/s41558-018-0072-6.

Finney DL, Doherty RM, Wild O, Huntrieser H, Pumphrey HC, Blyth AM (2014) Using cloud ice flux to parametrise large-scale lightning. Atmos Chem Phy 14:12665–12682. https://doi.org/10.5194/acp-14-12665-2014.

HouzeJr RA, Wilton DC, Smull BF (2007) Monsoon convection in the Himalayan region as seen by the TRMM precipitation radar. Quart J Roy Meteorol Soc 133(627):1389-1411.

Hurwitz MM, Calvo N, Garfinkel CI, Butler AH, Ineson S, Cagnazzo C, Manzini E, Peña-Ortiz C (2014) Extra-tropical atmospheric response to ENSO in the CMIP5 models. Clim Dyn 43(12):3367-3376.

Jeevanjee N, Romps DM (2018) Mean precipitation change from a deepening troposphere. Proc Nat Aca Sci 115(45):11465–11470. https://doi.org/10.1073/pnas.1720683115

Jourdain NC, Gupta AS, Taschetto AS, Ummenhofer CC, Moise AF, Ashok K (2013) The Indo-Australian monsoon and its relationship to ENSO and IOD in reanalysis data and the CMIP3/CMIP5 simulations. Clim Dyn 41(11-12) 3073-3102.

Kamra AK (1970) Effect of electric field on charge separation by the falling precipitation mechanism in thunder clouds. J Atmos Sci 27(8):1182-1185.

Kamra AK (1975) The role of electrical forces in charge separation by falling precipitation in thunderclouds. J Atmos Sci 32(1):143-157.

Kamra AK (1982a) Changes in concentrations of cloud and precipitation particles in the highly electrified regions of thundercloud. J Geophys Res 87:11215-11221

Kamra AK (1982b) Possible effect of the cloud electrification on the downdraft in thunderstorms. Geophys Res Lett 9:235-238.

Kamra AK, Bhalwankar RV, Sathe AB (1993) Onset of disintegration and corona in water drops falling at terminal velocity in horizontal electric fields. J Geophys Res 98:12901-12912.

Kamra AK, Pinki RK (2021) Regional variability in lightning activity over South Asia. Int J Clim 41(1):625-646.

Kandalgaonkar SS, Tinmaker MIR, Kulkarni JR, Nath ASHA, Kulkarni MK, Trimbake HK (2005) Spatio-temporal variability of lightning activity over the Indian region. J Geophys Res Atmos 110 D11108 .doi.10.1029/2004JD005631.

Krause A, Kloster S, Wilkenskjeld S, Paeth H (2014) The sensitivity of global wildfires to simulated past, present, and future lightning frequency. J Geophys Res Biogeos 119(3):312-322.

Kunkel KE, Karl TR, Brooks H, Kossin J, Lawrimore JH, Arndt D, Bosart L, Changnon D, Cutter SL, Doesken N, Emanuel K (2013) Monitoring and understanding trends in extreme storms: State of knowledge. Bull American Meteorol Soc 94(4):499-514.

Lambert FH, Webb MJ (2008) Dependency of global mean precipitation on surface temperature. Geophys Res Lett 35 L16706. https://doi.org/10.1029/2008GL034838.

Liu N, Liu C, Chen B, Zipser E (2020) What are the favorable large-scale environments for the highest-flash-rate thunderstorms on Earth?. J Atmos Sci 77:1583-1612.

Orville RE, Huffines G, Nielsen-Gammon J, Zhang R, Ely B, Steiger S, Phillips S, Allen S, Read W (2001) Enhancement of cloud-to-ground lightning over Houston, Texas. Geophys Res Lett 28(13):2597-2600.

Oulkar S, Siingh D, Saha U, Kamra AK (2019) Distribution of lightning in relation to topography and vegetation cover over the dry and moist regions in the Himalayas. J Earth Sys Sci 128: 180. https://doi.org/10.1007/s12040-019-1203-9.

Penki RK, Kamra AK (2013) The lightning activity associated with the dry and moist convections in the Himalayan regions. J Geophys Res Atmos 118:6246–6258. https://doi.org/10.1002/jgrd.50499.

Price C, Rind D (1994) Possible implications of global climate change on global lightning distributions and frequencies. J Geophys Res 99:10823-10831, doi:10.1029/94JD00019.

Qie X, Wu X, Yuan T, Bian J, Lu D (2014) Comprehensive pattern of deep convective systems over the Tibetan Plateau–South Asian monsoon region based on TRMM data. J. Clim, 27(17), 6612-6626.

Qie K, Qie X, Tian W (2021) Increasing trend of lightning activity in the South Asia region. Sci Bull 66:78-84. https://doi.org/10.1016/j.scib.2020.08.033

Ramesh Kumar P, Kamra AK (2012) Spatiotemporal variability of lightning activity in the Himalayan foothills. J Geophys Res 117 D2420. https://doi.org/10.1029/ 2012JD018246.

Ranalkar MR, Chaudhari HS (2009) Seasonal variation of lightning activity over the Indian subcontinent. Meteorol Atmos Phy 104(1):125-134.

Riahi K, Rao S, Krey V, Cho C, Chirkov V, Fischer G, Kindermann G, Nakicenovic N, Rafaj P (2011) RCP 8.5 A scenario of comparatively high greenhouse gas emissions. Clim Chan 109(1):33-57.

Romps DM, Seeley JT, Vollaro D, Molinari J (2014) Projected increase in lightning strikes in the United States due to global warming. *Science*, 346:851-854.

Romps DM, Charn AB, Holzworth RH, Lawrence WE, Molinari J, Vollaro D (2018) CAPE times P explains lightning over land but not the land-ocean contrast. Geophys Res Lett 12:623–12, 630. https://doi.org/10.1029/2018GL080267.

Roy I (2017) Indian Summer Monsoon and El Niño Southern Oscillation in CMIP5 Models: A Few Areas of Agreement and Disagreement. Atmos 8:154 https://doi.org/10.3390/atmos8080154.

Roy I, Tedeschi RG (2016) Influence of ENSO on regional ISM precipitation—local atmospheric influences or remote influence from Pacific. Atmos 7:25 https://doi.org/10.3390/atmos7020025.

Roy I, Tedeschi RG, Collins M (2017) ENSO teleconnections to the Indian summer monsoon in observations and models. Int J Clim 37:1794-1813. https://doi.org/10.1002/joc.4811.

Roy I, Gagnon AS, Siingh D (2019) Evaluating ENSO teleconnections using observations and CMIP5 models. Theor Appl Climatol 136:1085. https://doi.org/10.1007/s00704-018-2536-z.

Roy I., 2018. CMIP5 project and some results. In: Climate Variability and Sunspot Activity. Springer Atmospheric Sciences. https://doi.org/10.1007/978-3-319-77107-6_14.

Roy, I., Tedeschi, R.G., Collins, M., 2019. ENSO teleconnections to the Indian summer monsoon under changing climate, Int. J. Clim. 39, 3031-3042.

Saha U, Siingh D, Kamra AK, Galanaki E, Maitra A, Singh RP, Singh AK, Chakraborty S, Singh R (2017) On the association of lightning activity and projected change in climate over the Indian sub-continent. Atmos Res 183:173–190.

Saha K, NP Damase, T Banik, B Paul, S Sharma, BK De, A Guha (2019) Satellite based observation of lightning climatology over Nepal. J Earth Syst Sci 128:221, https://doi.org/10.1007/s12040-019-1239-x.

Seeley JT, Romps DM (2015) The effect of global warming on severe thunderstorms in the United States. J. Clim 28(6), 2443-2458.

Siingh, D., Ramesh Kumar, P., Kulkarni, M.N., Singh, R.P. and Singh, A.K. (2013) Lightning, convective rain and solar activity - over the South/Southeast Asia. Atoms. Res, 120–121:99–111. https://doi.org/10.1016/j.atmosres.2012.07.026.

Siingh D, Singh RP, Singh Ashok K, Kulkarni MN, Gautam AS, Singh AK (2011) Solar activity, lightning and climate. Sur Geophys 32:659–703, doi 10.1007/s10712-011-9127-1.

Siingh D, Buchunde PS, Singh RP, Nath A, Kumar S, Ghodpage RN (2014) Lightning and convective rain study at different parts of India. Atoms Res 137:35-48.

Siingh, D., Buchunde, P.S., Gandhi, H., Singh, R., Singh, S., Patil, M.N. and Singh, R.P. (2015) Lightning and convective rain over Indian peninsula and Indo-China peninsula. Adv Space Res 55:1085–1103. https://doi.org/10.1016/j.asr.2014.11.014.

Stolz DC, Rutledge SA, Pierce JR (2015) Simultaneous influences of thermodynamics and aerosols on deep convection and lightning in the tropics. J Geophy Res Atmos 120(12):6207-6231.

Stolz DC, Rutledge SA, Pierce JR, Van den Heever SC (2017) A global lightning parameterization based on statistical relationships among environmental factors, aerosols, and convective clouds in the TRMM climatology. J Geophy Res Atmos 122(14):7461-7492.

Stolzenburg M, Rust WD, Smull BF, Marshall TC (1998) Electrical structure in thunderstorm convective regions: 1. Mesoscale convective systems. J Geophy Res Atmos 103(D12):14059-14078.

Taylor KE, Stouffer RJ, Meehl GA (2012) An Overview of CMIP5 and the Experiment Design. Bull. Amer Meteor Soc 93:485-498.

Tippett MK, Lepore C, Koshak WJ, Chronis T, Vant-Hull B (2019) Performance of a simple reanalysis proxy for US cloud-to-ground lightning. Int J Clim 39(10):3932-3946.

Tost H, Jöckel P, Lelieveld J (2007) Lightning and convection parameterisations–uncertainties in global modeling. Atmos Chem Phys 7(17):4553-4568.

Toumi R, Qie X (2004) Seasonal variation of lightning on the Tibetan Plateau: A Spring anomaly?. Geophys Res Lett 31(4).

Trapp RJ, Diffenbaugh NS, Brooks HE, Baldwin ME, Robinson ED, Pal JS (2007a) Changes in severe thunderstorm environment frequency during the 21st century caused by anthropogenically enhanced global radiative forcing. Proc. Nat. Aca. Sci, 104(50), 19719-19723.

Trapp RJ, Halvorson BA, Diffenbaugh NS (2007b) Telescoping, multi model approaches to evaluate extreme convective weather under future climates. J. Geophy. Res.: Atmos, 112, D20109, doi:10.1029/2006JD008345.

Tyagi B, Krishna VN, Satyanarayana ANV (2011) Study of thermodynamic indices in forecasting pre-monsoon thunderstorms over Kolkata during STORM pilot phase 2006-2008. Nat Hazards 56:681–698. doi:10.1007/s11069-010- 9582-x.

Tyagi B, Satyanarayana ANV, Vissa NK (2013) Thermodynamical structure of atmosphere during pre-monsoon thunderstorm season over Kharagpur as revealed by STORM Data. Pure Appl Geophys 170:675–687. doi:10.1007/s00024-012-0566-5.

Vonnegut B (1963) Some facts and speculations concerning the origin and role of thunderstorm electricity. Meteorol Monogrs 27:224–41

Williams ER, Weber ME, Orville RE (1989) The relationship between lightning type and convective state of thunder clouds. J Geophys Res 94: 13213–13220.

Williams ER, Rutledge SA, Geotis SG, Renno N, Rasmussen E, Rickenbach T (1992) A radar and electrical study of tropical "hot towers". J Atmos Sci 49:1386-1395.

Williams ER, Rosenfeld D, Madden N, Gerlach J, Gears N, Atkinson L, Dunnemann N, Frostrom G, Antonio M, Biazon B, Camargo R, Franca H, Gomes A, Lima M, Machado R, Manhaes S, Nachtigall L, Piva H, Quintiliano W, Machado L, Artaxo P, Roberts G, Renno N, Blakeslee R, Bailey J, Boccippio D, Betts A, Wolff D, Roy B, Halverson J, Rickenbach T, Fuentes J, Avelino E (2002) Contrasting convective regimes over the Amazon: Implications for cloud electrification, J Geophys Res 107(D20) 8082 doi:10.1029/2001JD000380.

Wu XK, Qie XS, Yuan T (2013) Regional distribution and diurnal variation of deep convective systems over the Asian monsoon region. Sci. China Earth Sci 56:843–854, doi:10.1007/s11430-012-4551-8.

Wu XK, Qie XS, Yuan T, Li J (2016) Meteorological regimes of the most intense convective systems along the southern Himalayan front. J Clim 29:4383-4393. doi: 10.1175/JCLI-D-14-00835.1

Zipser EJ, Lutz KR (1994) The vertical profile of radar reflectivity of convective cells: A strong indicator of storm intensity and lightning probability?. Mon Weat Rev 122(8):1751-1759.

Zipser EJ, Cecil DJ, Liu C, Nesbitt SW, Yorty DP (2006) Where are the most intense thunderstorms on Earth? Bull Ameri Meteorol Soc 87(8):1057-1072.

Legends

Figure 1(a) Spatial distribution of lightning flash rate (LFR) (flashes km^{-2} day^{-1}) for pre-monsoon (MAM) (March, April, May) season over the south/southeast Asia using observed data from Lightning Imaging Sensor (LIS)/ Optical Transient Detector (OTD) mounted on the Tropical Rainfall Measuring Mission (TRMM) satellite (top left), model ensemble data (top right) and nine GCMs, CMIP5 model ensemble data (bottom three rows).

Figure 1(b) Same as Figure 1a, but for monsoon (JJAS) (June, July, August, September) season.

Figure 1(c) Same as Figure 1a, but for post-monsoon (ON) (October-November) season.

Figure 1(d) Same as Figure 1a, but for winter (DJF) (December-January-February) season.

Figure 2. Same as Figure 1, but for annual mean.

Figure 3.Scatter plot between the monthly-averaged LFR from observed data and ensemble mean of GCMs', CMIP5 model data for the historic period 1995-2006over the south/southeast Asia.

Figure 4. Spatial distribution of lightning flash rate (LFR) (flashes km^{-2} day^{-1}) of annual mean, using nine different CMIP5 model data for the future period 2079-2088 over the south/southeast Asia. The top left panel of the figure is model ensemble and the top right panel of the figure is for the (RCP– historic) data.

Figure 5. Spatial distribution of lightning flash rate (LFR) (flashes km^{-2} day^{-1}) of (a) pre-monsoon, (b) monsoon, (c) post-monsoon and (d) winter season, using nine different CMIP5 model data for the future period 2079-2088 over the south/southeast Asia. The left column of the figure is for the model ensemble and right column for the (RCP – historic) data.

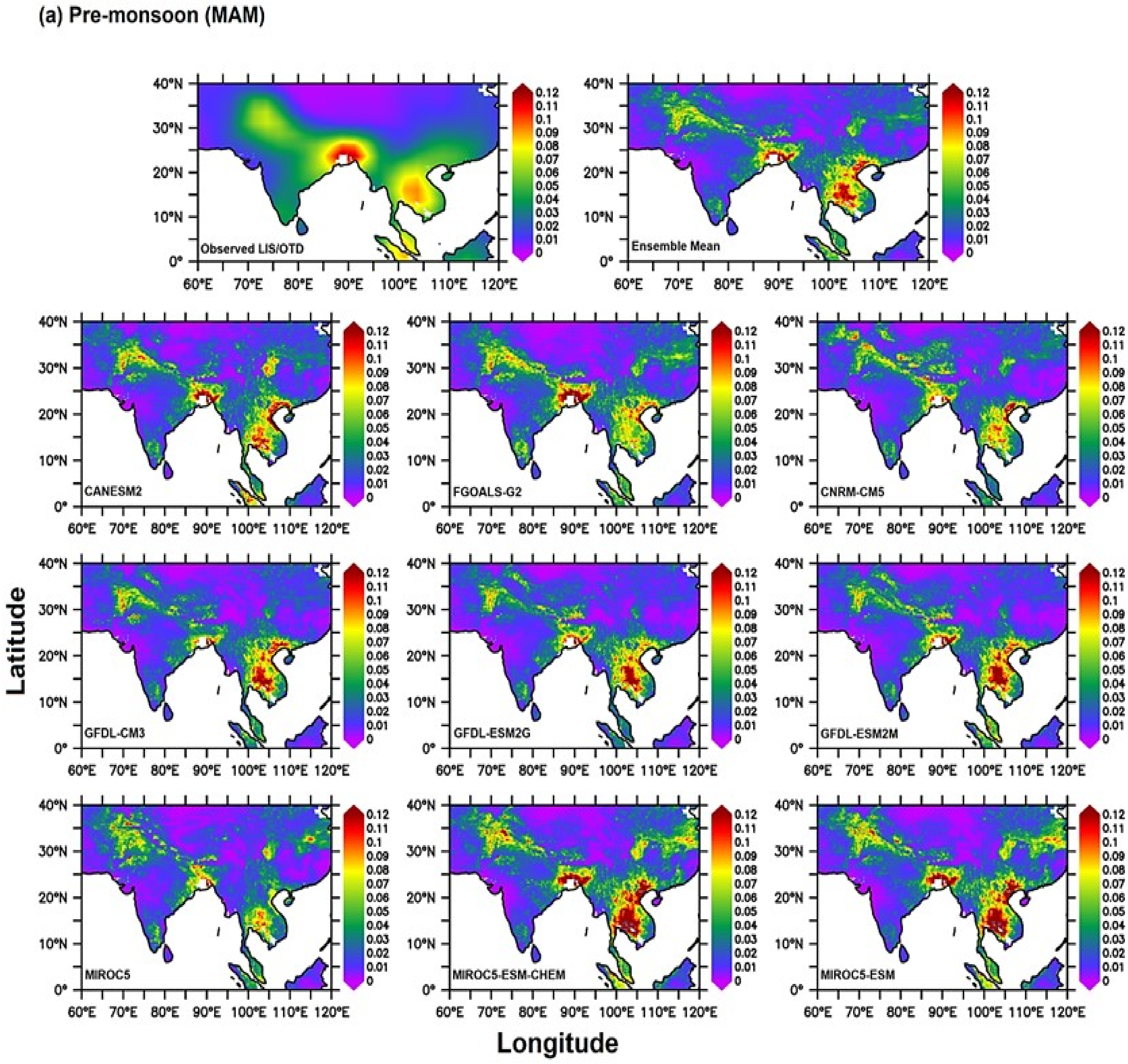

Figure 1(a). Spatial distribution of lightning flash rate (LFR) (flashes km^{-2} day^{-1}) for pre-monsoon (MAM) (March, April, May) season over the south/southeast Asia using observed data from Lightning Imaging Sensor (LIS)/ Optical Transient Detector (OTD) mounted on the Tropical Rainfall Measuring Mission (TRMM) satellite (top left), model ensemble data (top right) and nine GCMs, CMIP5 model data (bottom three rows).

(b) Monsoon (JJAS)

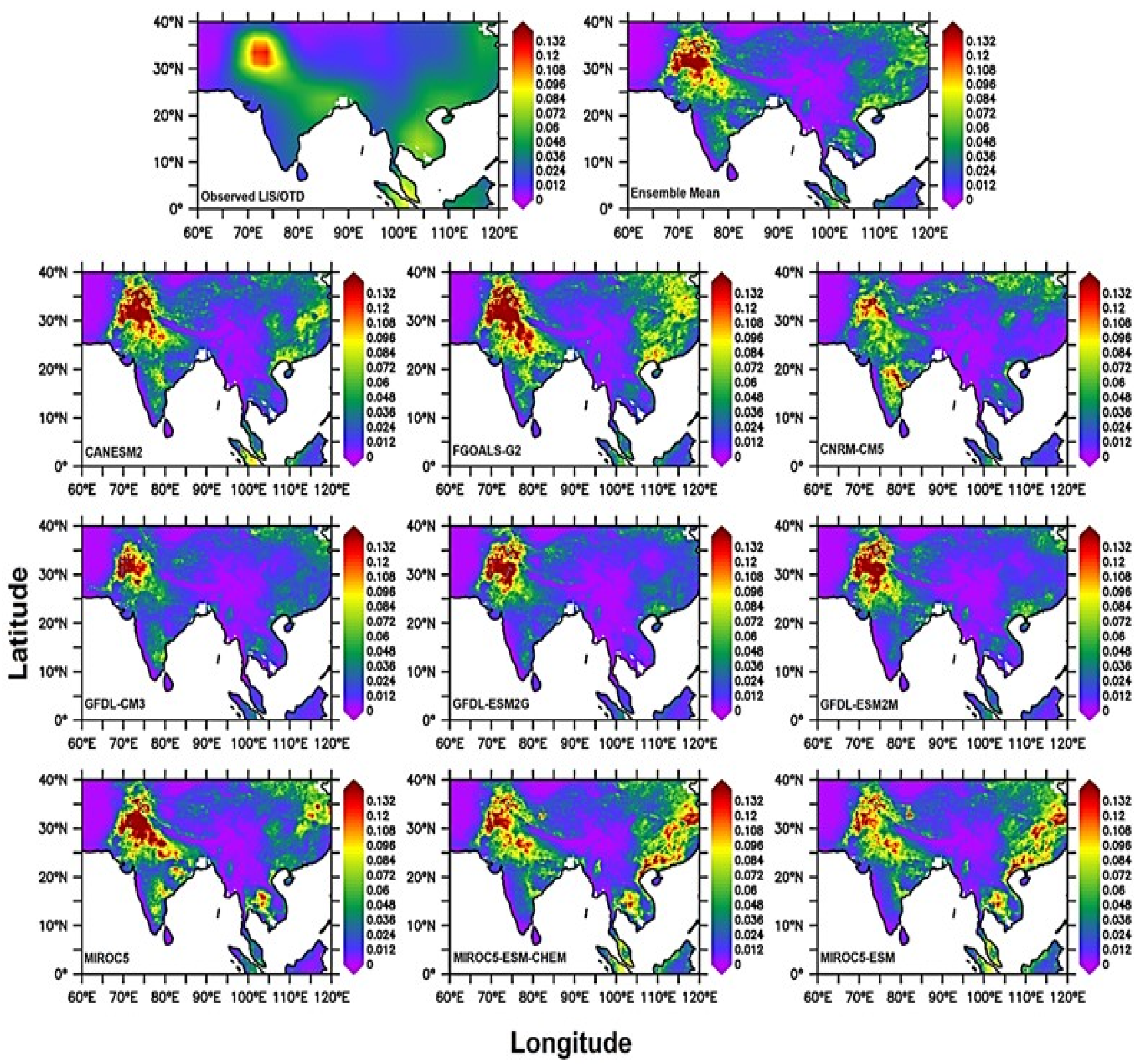

Figure 1(b). Same as Fig 1a, but for monsoon (JJAS) (June, July, August, September) season

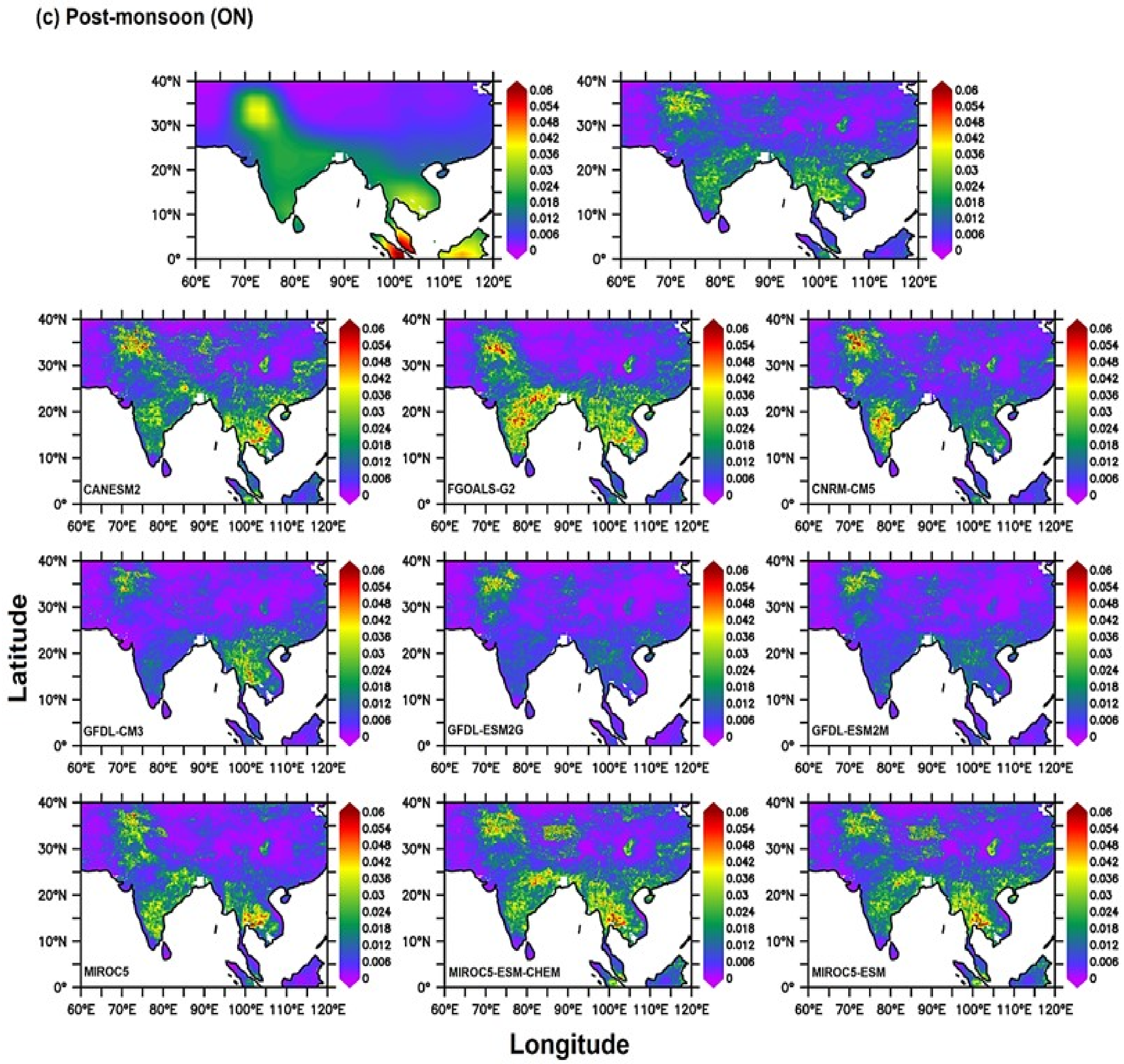

Figure 1(c). Same as Figure 1a, but for post-monsoon (ON) (October-November) season.

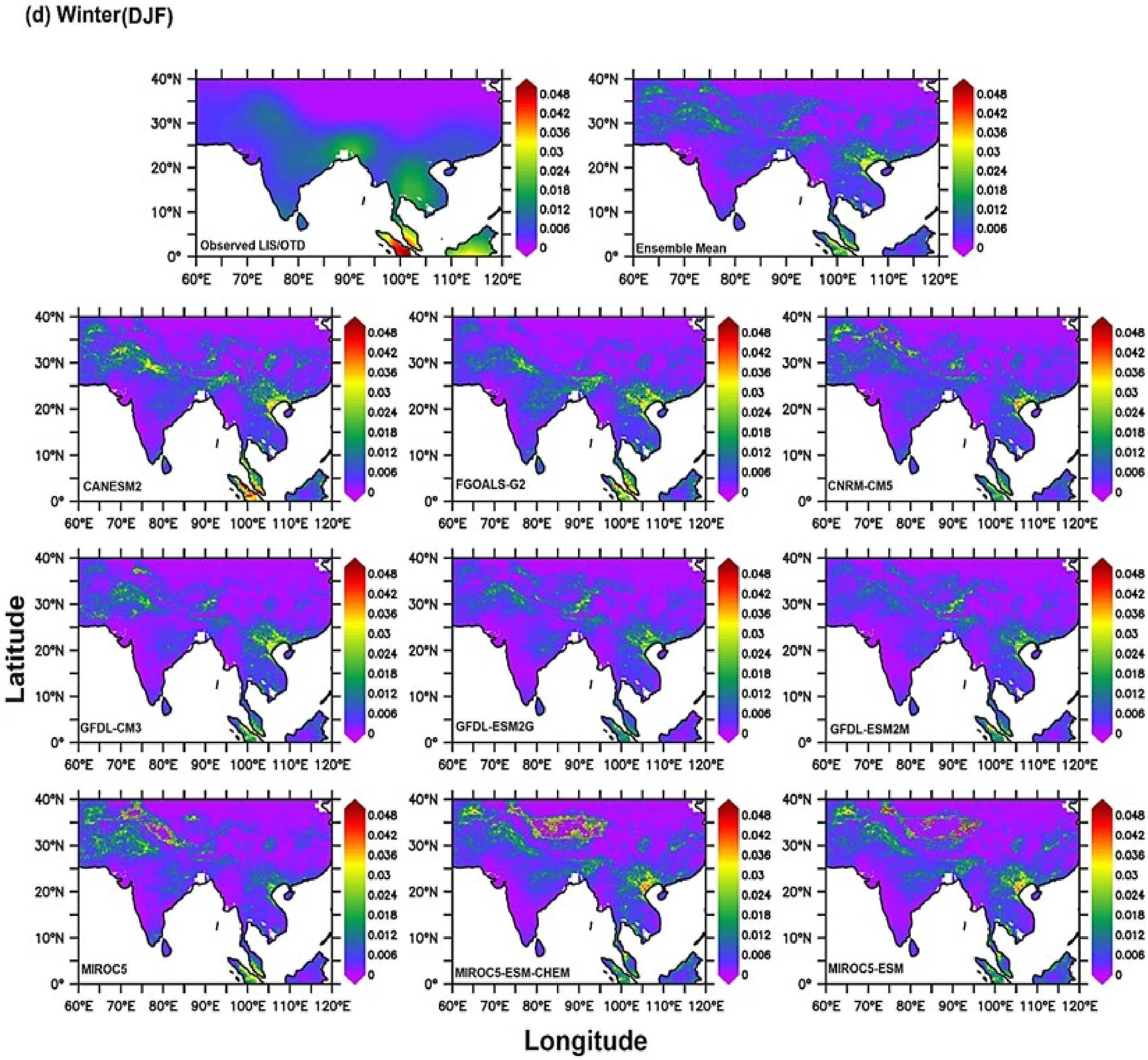

Figure 1(d). Same as Figure 1a, but for winter (DJF) (December-January-February) season.

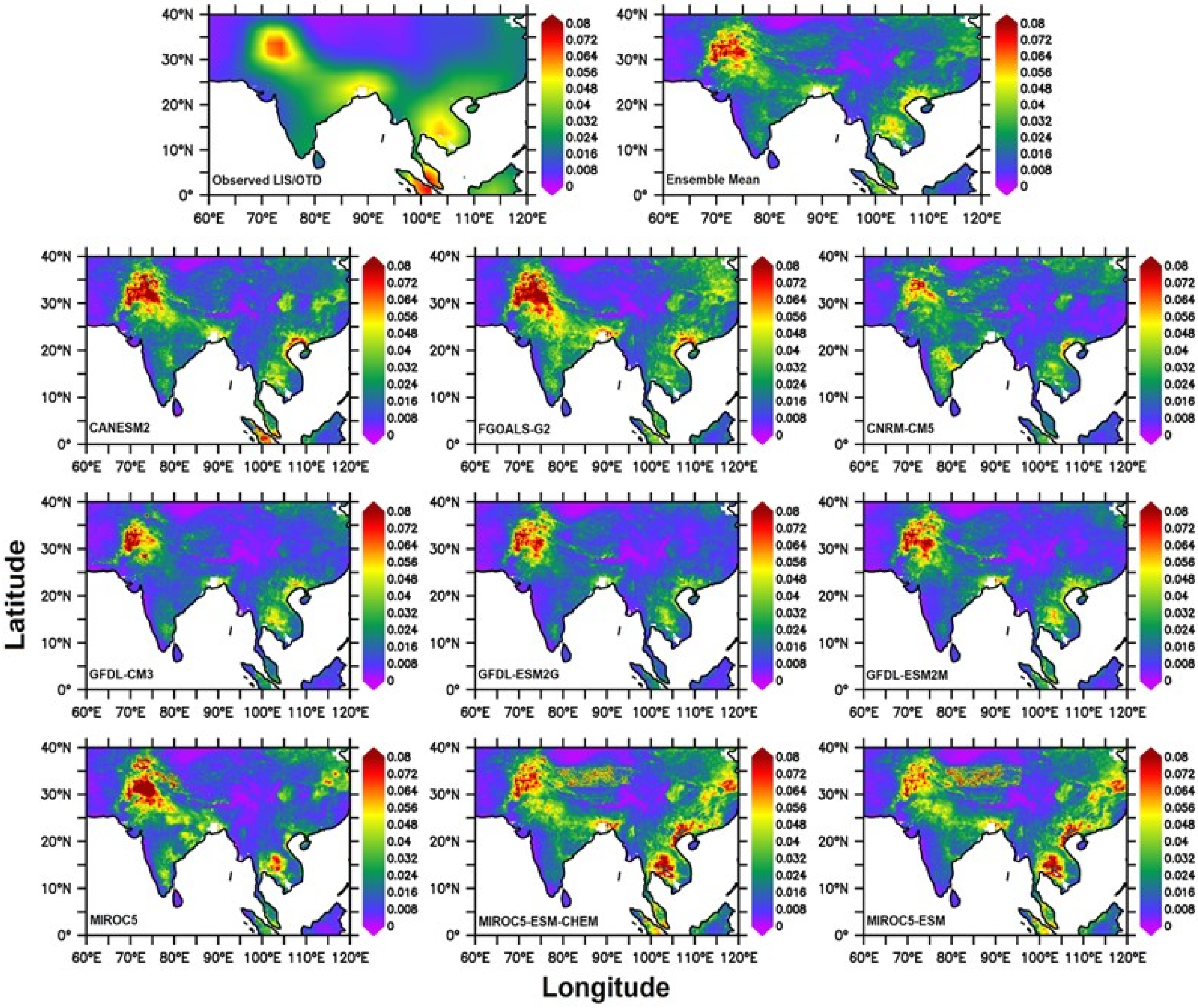

Figure 2. Same as Figure 1, but for annual mean.

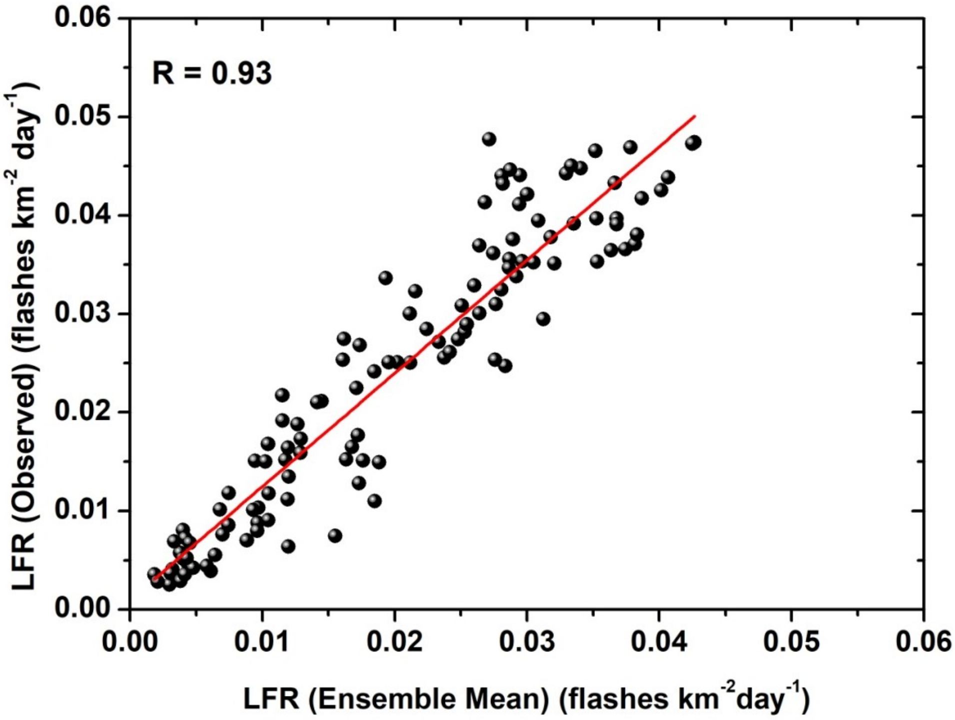

Figure 3. Scatter plot between the monthly-averaged LFR from observed data and ensemble mean of GCMs', CMIP5 model data for the historic period 1995-2006 over the south/southeast Asia.

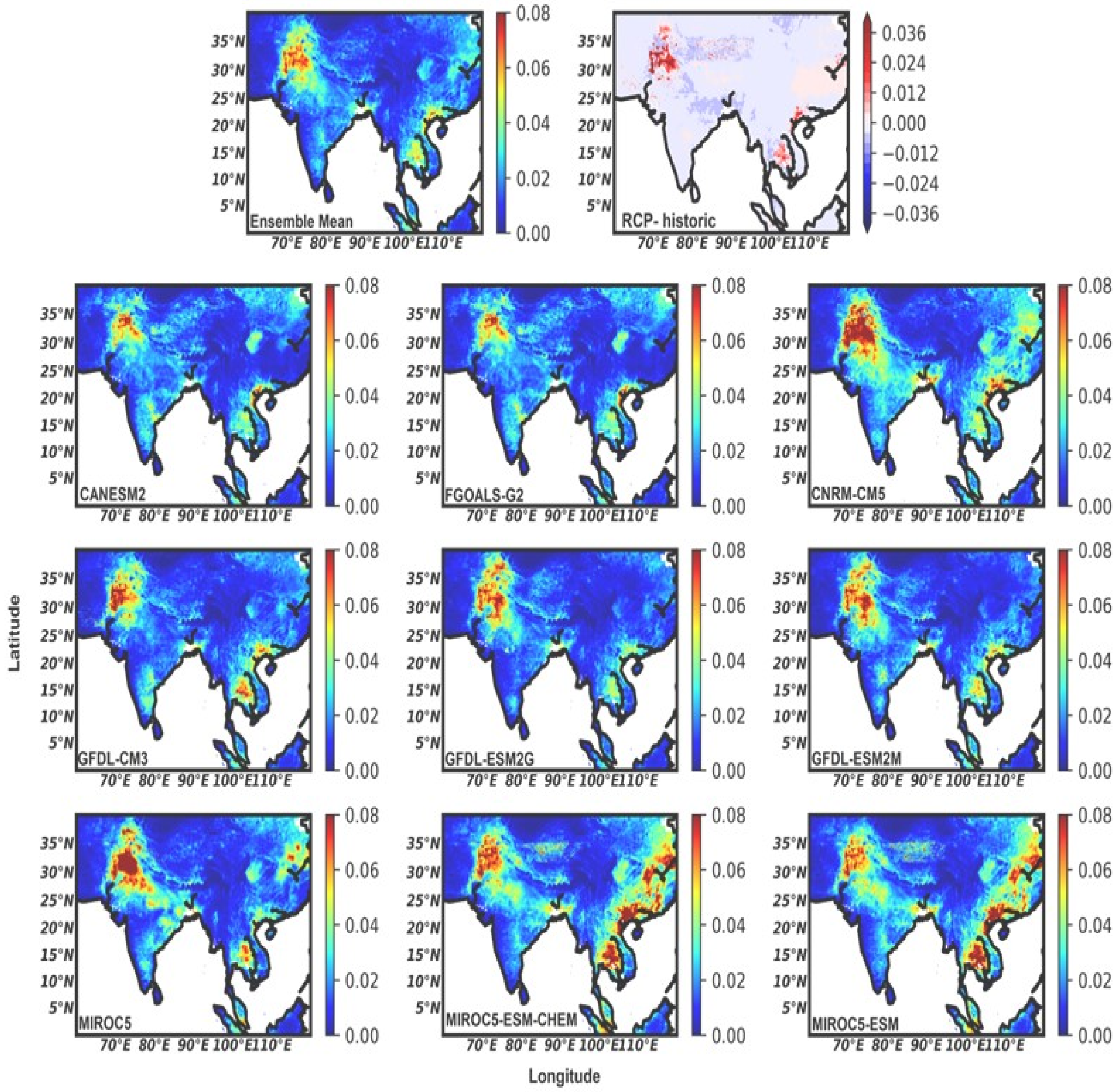

Figure 4. Spatial distribution of lightning flash rate (LFR) (flashes km^{-2} day^{-1}) **of annual mean,** using nine different CMIP5 model data for the future period 2079-2088 over the south/southeast Asia. The top left panel of the figure is model ensemble and the top right panel of the figure is for the (RCP8.5 – historic) data.

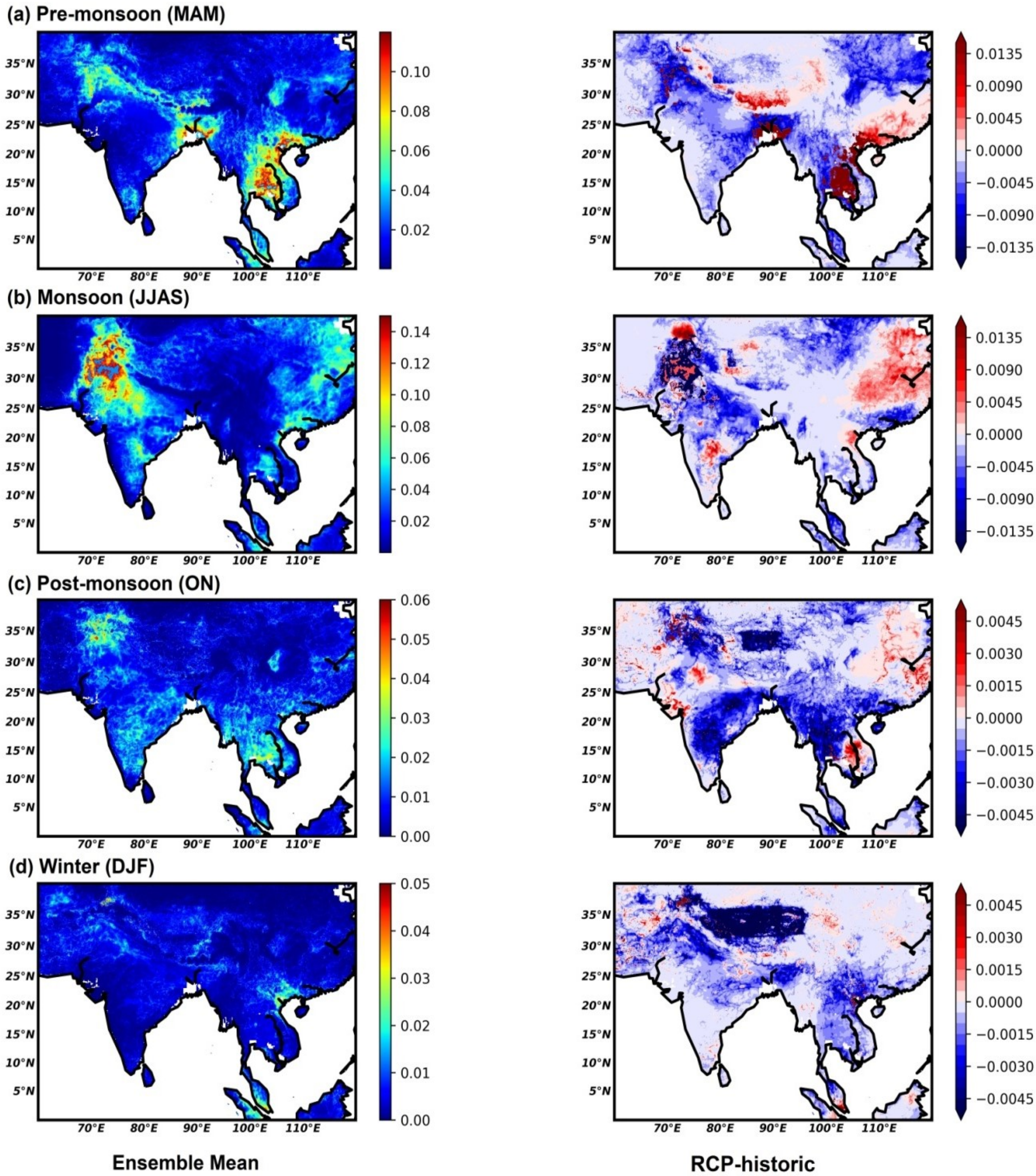

Figure 5. Spatial distribution of lightning flash rate (LFR) (flashes km^{-2} day^{-1}) of (a) pre-monsoon, (b) monsoon, (c) post-monsoon and (d) winter season, using nine different CMIP5 model data for the future period 2079-2088 over the south/southeast Asia. The left column of the figure is for the model ensemble and right column for the (RCP8.5 – historic) data.

Table 1: Correlation Coefficients (CC) between the observed Lightning Flash Rate (LFR) and proxy (I), and observed LFR and various models (II) derived during pre-monsoon, monsoon, post-monsoon, winter season and annual mean for the historic period, 1996-2005.

	C.C.									
	Pre-monsoon		**Monsoon**		**Post-monsoon**		**Winter**		**Annual**	
GCMs	I	II	I	II	I	II	I	II	I	II
CANESM2	0.82	0.81	0.77	0.70	0.71	0.93	0.81	0.93	0.86	0.94
CNRM-CM5	0.83	0.78	0.62	0.68	0.77	0.73	0.55	0.82	0.80	0.83
FGOALS-G2	0.77	0.87	0.78	0.72	0.79	0.71	0.56	0.79	0.84	0.92
GFDL-CM3	0.86	0.75	0.70	0.79	0.77	0.78	0.65	0.93	0.70	0.93
GFDL-ESM2G	0.80	0.74	0.77	0.80	0.79	0.89	0.76	0.95	0.71	0.94
GFDL-ESM2M	0.70	0.81	0.78	0.79	0.75	0.89	0.71	0.96	0.74	0.94
MIROC5	0.87	0.86	0.53	0.70	0.76	0.88	0.70	0.72	0.81	0.77
MIROC-ESM-CHEM	0.82	0.81	0.55	0.78	0.62	0.66	0.65	0.62	0.75	0.72
MIROC-ESM	0.81	0.82	0.34	0.75	0.58	0.51	0.68	0.59	0.75	0.77

Table 2: Percent changes in LFR, precipitation (P_r), evaporation (E_v) and air temperature (T) projected for 2079-2088 as compared to the historic period 1996-2005 by various GCMs in RCP8.5 scenario.

GCMs	**ΔLFR (%)**	**ΔP_r (%)**	**ΔE_v (%)**	**ΔT(°C)**
CAN-ESM2	2.21	14.57	4.72	4.68
FGOALS G 2	22.02	8.97	10.26	1.93
CNRM_CM5	4.42	10.30	12.10	2.47
GFDL_CM3	15.95	19.31	18.52	4.30
GFDL_ESM 2G	6.25	5.36	5.95	3.49
GFDL_ESM 2M	10.01	6.13	3.76	3.28
MIROC5	-1.62	18.31	13.57	3.37
MIROC_ESM_CHEM	3.18	9.42	12.75	4.41
MIROC_ESM	-1.64	7.90	10.38	3.99
Mean	**6.75**	**11.14**	**10.23**	**3.54**

Table 3a: Same as Table 2, but for the projected period (2051-60) instead of 2079-2088.

GCMs	ΔLFR (%)	ΔP_r (%)	ΔE_v (%)
CAN-ESM2	3.08	2.81	5.02
FGOALS G 2	10.41	6.32	1.74
CNRM_CM5	5.50	5.15	4.53
GFDL_CM3	7.02	8.97	8.87
GFDL_ESM 2G	1.79	1.92	1.85
GFDL_ESM 2M	4.04	3.55	2.14
MIROC5	-2.05	11.39	4.97
MIROC_ESM_CHEM	9.20	4.71	4.50
MIROC_ESM	0.15	5.57	5.01
Mean	**4.30**	**5.60**	**4.29**

Table-3b: Percent changes in LFR, precipitation (P_r) and evaporation (E_v) projected for 2079-2088 as compared to the historic period 1996-2005 by various GCMs*, in the RCP4.5 scenario.

GCMs	ΔLFR (%)	ΔP_r (%)	ΔE_v (%)
CAN-ESM2	8.08	4.63	7.19
FGOALS G 2	14.87	7.96	3.77
CNRM_CM5	1.96	7.86	3.45
GFDL_CM3	-	-	-
GFDL_ESM 2G	4.01	2.14	2.27
GFDL_ESM 2M	6.36	5.51	2.34
MIROC5	-0.85	17.41	10.09
MIROC_ESM_CHEM	4.93	8.09	7.02
MIROC_ESM	3.48	5.97	6.60
Mean	**5.36**	**7.32**	**5.34**

*Model GFDL_CM3 does not have all required parameters in RCP4.5 scenario and hence omitted.